Smart Structures and Systems, *Vol. 28, No. 1 (2021) 29-41*
https://doi.org/10.12989/sss.2021.28.1.029

A study of a new hybrid vibration energy harvester based on broadband-multimode

Bing Chen*[1], Shiqing Li [1], Xiaolei Tang [1] and Lijie Zhang [2]

[1] *School of Mechanical Engineering, University of Science and Technology Beijing, Beijing 100083, China*
[2] *China North Research Institute, Beijing, 100072, China*

(*Received December 28, 2019, Revised April 22, 2021, Accepted April 29, 2021*)

Abstract. To improve the energy conversion efficiency and working frequency bandwidth of a single frequency piezoelectric vibration energy harvester, a new type of hybrid vibration energy harvester is developed which is combined with the mechanism of piezoelectric and electromagnetic energy conversion. The system comprises of a PZT cantilever beam, an elastic suspended magnetic mass, a magnet block attached to the end of the cantilever beam and a resonator. The addition of resonator can not only increase the mode, but also adjust the frequency of harvester flexibly. Nonlinear magnetic force of magnet block not only broadens the frequency band and improves the output performance of the system, but also changes the resonant frequency to make the harvester have better adjustable performance. On this basis, an improved electromechanical coupled analytical model of continuum is proposed which can be solved by the Runge-Kutta algorithm and the influence of different factors (the mass and spring stiffness of the resonator, as well as the electromechanical coupling coefficient, electromagnetic coupling coefficient, magnet mass and magnetic flux) on the output are analyzed. According to the prototype of the vibration energy harvester developed, an experimental system was built. The performance of the independent and hybrid energy harvesters is evaluated by experimental and analytical methods. The peak output voltage of the piezoelectric part was about 4 times that of the electromagnetic part. The peak output current of the electromagnetic part is about 30 times that of the piezoelectric part. The study results show that the proposed new hybrid vibration energy harvester can achieve a wider frequency range and multi-modal vibration energy harvesting. In addition, the bandwidth and power of the harvester can be dynamically adjusted by changing the resonator or electromechanical coupling coefficient, and the bandwidth of the harvester can also be adjusted by changing the quality and characteristics of the magnet.

Keywords: continuum; electromechanical coupling model; multimode; piezoelectric-electromagnetic mixing; resonator

1. Introduction

With the extensive development of portable electronic equipment, MEMS and wireless sensor networks, automatic sensing and communication are required across many fields (Matiko *et al*. 2013, Hannan *et al*. 2014). Engineering can be improved with the development of low-power wireless sensor, but how to supply power without using dry cell batteries which need to be repeatedly charged and discharged is of fundamental interest. One of the effective solutions proposed by the academic is to harvest energy from working environment (Mutashar *et al*. 2013, Beeby *et al*. 2006). This demand attracted the attentions of many researchers/academics for energy harvesting researches in the last decade (Matiko *et al*. 2013, Beeby *et al*. 2006, Wang 2016, Wang and Xiao 2013, Ab Rahman *et al*. 2013).

Many early studies on energy harvesting were based on single-frequency harvesters (Roundy and Wright 2004, Siddique *et al*. 2015). As we all know, the vibration frequency is unstable in natural environment, and the vibration energy is mostly distributed in a fixed broadband. It is difficult to produce resonance for a single resonant frequency piezoelectric energy harvester, which will inevitably lead to low efficiency of electromechanical energy conversion of the harvester (Siddique *et al*. 2015).

Therefore, more and more attention has been paid to different methods of obtaining energy from multi-mode and wideband frequency vibration (Jaber *et al*. 2016), such as multi-modal technology (Yang *et al*. 2009), resonance tuning technology (Huang and Lin 2012) and nonlinear harvesting technology (Siddique *et al*. 2015, Jaber *et al*. 2016, Sari *et al*. 2008, Zhou *et al*. 2016, Leng *et al*. 2017).

Energy acquisition based on piezoelectric effect mostly adopts cantilever beam and single frequency excitation, which is the most basic energy acquisition method based on resonance. But the environmental vibration is complex and changeable, thus, the best performance of energy harvesters is always limited to excitation at its natural frequency (Varoto and Mineto 2014). To solve the conflict of narrow frequency band and small output power, piezomagnetoelastic systems are being studied more and more as broadband energy harvesters. Erturk *et al*. (2009) introduced a piezomagnetoelastic device whose experimental performance qualitative agreement with the theory. Compared with the conventional case without magnetic buckling, it is proved that the piezoelectric

*Corresponding author, Professor,
E-mail: bingchen9803@ustb.edu.cn

http://www.techno-press.org/?journal=sss&subpage=7
ISSN: 1738-1584 (Print), 1738-1991 (Online)

electromagnetic elastic structure can improve the advantages of the broadband generator. Zhao and Erturk (2009). conducted numerical and experimental studies on the broadband random vibration energy acquisition of monostable and bistable piezoelectric cantilever beams. The study shows that under wide-band random excitation, the bistable energy harvester can be preferred only if it is designed to work under known excitation intensity.

Electromagnetism has also attracted more and more attention in energy harvesting. When the coil moves relative to the magnet, electricity is generated according to Faraday's law. Different shapes of cantilever beam and different magnets with different coil size are being used (Cannarella *et al*. 2011). Rajarathinam and Ali (2018) developed a broadband hybrid energy harvester that combines piezoelectric and electromagnetic effects. And the electromechanical coupling coefficient and the stiffness of the cantilever can affect the output power. Mann and Sims (2009) proposed the energy harvester using magnetic levitation to generate a tunable oscillator. The nonlinearity of magnetic levitation can produce large oscillations. The addition of magnetic force gives variable factors to the output characteristics of the energy harvester. Some are easy to adjust, such as the mass and position of the magnet block. However, some are harder to change, such as damping level.

Although the nonlinear response can generate frequencies of broadband random, it can only work in certain bandwidth environments. In fact, the source of vibration in the environment is usually random. Therefore, traditional a single-degree-of-freedom energy harvester is inefficient. To improve energy harvesting efficiency, Researchers have tried to design and invent multimodal energy harvesters so that the energy harvester can excite multiple voltage peaks within a frequency range to make greater use of the energy generated by vibration. Zhou *et al*. (2011) proposed a piezoelectric energy harvester which can increase the bandwidth and energy of ambient vibration by using multimode amplifier. Tao *et al*. (2011) added electromagnetic force to form the two-degree-of-freedom (2DOF) harvester which is more efficient than the ordinary one-degree-of-freedom (1DOF) harvester. To adapt to the diversity of environmental frequencies, the combination of multimodal technology and nonlinear force is often used in energy harvesters. Shen *et al*. (2015) proposed a piezomagnetoelastic beam array structure for vibration energy harvester. Compared with conventional harvesters, the nonlinear vibration energy harvesters produce larger power in several excitation frequency ranges. However, such beam array often takes up more space. Although the structure design combines nonlinear magnetic force and multimode, the multimode mode is large in volume and inconvenient in frequency modulation.

In addition to experiments and simulations, numerical solutions are often used to analyze the frequency characteristics and output of piezoelectric energy harvesting. Zhao and Erturk (2013) presented electroelastic modeling and numerical solutions which can be used as a more accurate alternative to single-degree-of-freedom solutions for wideband random energy harvesting. Kumar *et al*. (2015) proposed the mathematical model for the wideband piezoelectric elastic energy harvester. The electromechanical coupling equations are derived to describe the nonlinear dynamics. Also, the effect of base magnetic separation and the intensity of magnetic head are reported to confirm that once the system experiences the inter-well oscillation, it will gain more electrical energy. Ali *et al*. (2010) derived the approximate formula of the optimal electrical parameter which maximizes the average harvested power. The existing numerical analysis is based on dynamics, electromagnetism and other fields, and has strong theoretical support.

This paper presents a new type of hybrid energy harvester which is composed of a PZT cantilever beam, an elastic suspended magnetic mass, a magnet block and a resonator. The resonator can not only increase the modal number of the hybrid harvester, but also adjust the resonant frequency and increase the bandwidth. The piezoelectric beam collector and magnet are coupled to form a bistable system, and such nonlinear magnetic interaction can not only broaden the frequency band and improve the output performance of the system, but also change the resonance frequency, which makes the harvester has a more flexible adjustable performance. In this case, an improved electromechanical coupling continuum analysis model was proposed on the basis of Zhao's work (Zhao and Erturk 2013), and the Runge-Kutta algorithm was used to conduct quantitative numerical analysis through MATLAB, which was mutually verified with the experimental results. And different from the research work of Ali *et al*. (2010), the influence of more certain and uncertain factors, including mass, stiffness and coefficient, on the output are all analyzed.

The paper shows that the hybrid energy harvester can achieve multi-modal vibration energy collection in a wider frequency band. In addition, the bandwidth and power of the harvester can be dynamically adjusted by the resonator or electromechanical coupling coefficient, and the bandwidth can be adjusted by changing the quality factor and characteristics of the magnet.

In this paper, the numerical expression of the harvester is analyzed and modelling of the harvester is described. The energy harvester is numerically analyzed being used MATLAB and compared to that of independent harvesters. The numerically simulation results are in good agreement with the experimental results. Finally, conclusions and results are discussed.

2. Analytical modeling of the hybrid harvester

The hybrid energy harvester is shown in Fig. 1. It consists of an elastic suspended magnetic mass, a resonator, a PZT cantilever beam and a magnet block attached on the cantilever beam. When the device vibrates with the foundation, the cantilever beam undergoes a strain, which generates electrical energy through the piezoelectric transduction, while the copper coil collects energy through electromagnetic induction by cutting the oscillating magnetic field flux lines. The magnet block adhered to the

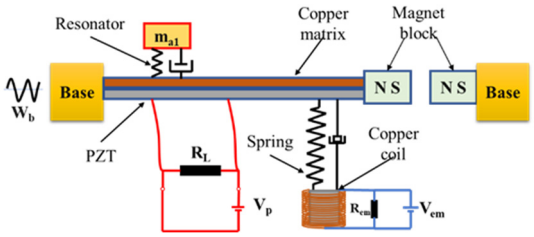

Fig. 1 Broadband-multimodal hybrid energy harvester (BMHEH)

free end is subjected to a nonlinear magnetic force, and the resonator consisting of a spring and a mass block increases the number of piezoelectric cantilever modes and reduce the influence of the strain node. Multiple frequencies of the energy harvester are matched with the excitation frequencies to improve the transducer efficiency. So, the system is referred to as a broadband-multimodal hybrid energy harvester (BMHEH).

The resonator as shown in Fig. 1 is a spring-mass vibration subsystem, where m_{a1} represents the mass of the resonator, w_b is the base displacement. The electromagnetic (EM) portion is suspended by springs at the end of the cantilever. The magnetic exciter (MOE) consists of a magnet block mounted on the end of the cantilever and a magnetic block fixed on the base.

As shown in Fig. 1, the resistances of the external circuit of the piezoelectric and the electromagnetic portion are R_p and R_{em}, and the voltage generated is V_p and V_{em} respectively.

2.1 Electromechanical coupled continuum model

Erturk and Inman (2008) established a mathematical model of the piezoelectric cantilever beam. However, after adding a resonator and a magnetic exciter to the cantilever beam, and introducing an electromagnetic energy harvester, the electromechanical coupling continuum model and its related characteristics need further study. The system shown in Fig. 1 can be illustrated by an electromechanical coupled continuum model, and the motion of the device under basic excitation is shown in Fig. 2.

Fig. 2(a) shows the force and motion of the cantilever beam, where x_a denotes the horizontal displacement of the point of junction between the resonator 1 and the cantilever beam to the fixed end of the cantilever, x_l is the horizontal displacement from the end of the cantilever to the fixed end, w_b represents the displacement of the fixed end of the cantilever relative to the foundation, f_{a1} represents the force of the resonator 1 on the cantilever beam, f_{a2} is the force exerted by the suspension spring of the electromagnetic (EM) part on the end of the cantilever, and f_m is the force exerted by the end magnet on the cantilever. Fig. 2(c) shows the force and motion of the electromagnetic (EM) part, $\mathrm{w}(x_l)$ is the absolute displacement of the end of the cantilever, z_{a2} is the displacement of the magnet block of the electromagnetic (EM) part relative to the cantilever, and $-f_{a2}$ is the counterforce of the electromagnetic (EM) part subjected to the cantilever. Fig. 2(d) shows the force and motion of the magnetic exciter (MOE), d denotes the horizontal distance between two magnetic blocks, $\mathrm{w}(x_l)$ denotes the displacement of the end of the cantilever relative to the foundation, F denotes the magnetic force between two magnetic blocks, F_n denotes the vertical component of the nonlinear magnetic force, and $-f_m$ denotes the reaction force of the cantilever for the magnet.

When establishing the kinematics equations and governing equations of the BMHEH system, it is necessary to introduce the Dirac function to write the concentrated force f_{a1}, f_m, and f_{a2} of the resonator, the end magnet, and the end spring respectively received by the cantilever beam into the form of distributed force.

$$\begin{cases} f_{a1} = \delta(x - x_a) f_{a1} \\ f_m = \delta(x - x_l) f_m \\ f_{a2} = \delta(x - x_l) f_{a2} \end{cases} \tag{1}$$

The cantilever beam is a continuum (Erturk and Inman 2008). Due to the continuum vibration theory, the equation of motion of the piezoelectric cantilever beam element in the Z-axis direction can be obtained as follows

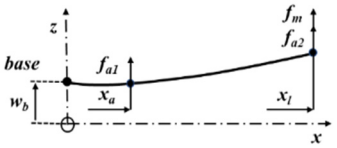

(a) Motion of the piezoelectric cantilever

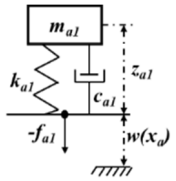

(b) Motion of the resonator

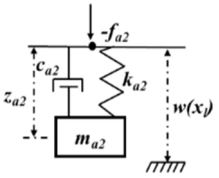

(c) Motion of EM

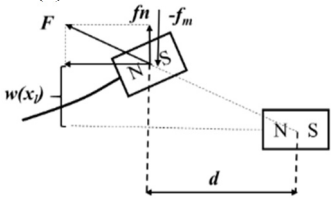

(d) Motion of MOE

Fig. 2 The motion model of BMHEH under translational excitation

$$\rho_l \frac{\partial^2 w_{rel}(x)}{\partial t^2} + \frac{\partial^2}{\partial x^2}\left[YI\frac{\partial^2 w_{rel}(x)}{\partial x^2} + c_s I\frac{\partial^3 w_{rel}(x)}{\partial x^2 \partial t} + \theta V_p\right] = -\rho_l \frac{\partial^2 w_b}{\partial t^2} + \delta(x - x_a)f_{a1} + \delta(x - x_l)f_m + \delta(x - x_l)f_{a2} \tag{2}$$

where ρ_l indicates the mass per unit length of the piezoelectric cantilever; YI indicates the bending stiffness; c_s indicates the damping coefficient; I indicates the sectional moment of inertia of the piezoelectric cantilever; θ indicates the electromechanical coupling coefficient; $w_{rel}(x)$ indicates the relative displacement of the piezoelectric cantilever to the foundation, and V_p indicates the output voltage of the piezoelectric portion (PHH).

The equations of motion of the resonator mass block ma1 and the electromagnetic mass block m_{a2} can be obtained from Figs. 2 (b) and (c), as shown in formula 3

$$\begin{cases} m_{a1}\ddot{z}_{a1} + c_{a1}\dot{z}_{a1} + k_{a1}z_{a1} = m_{a1}(\ddot{w_{rel}}(x_a) + \ddot{w}_b) \\ m_{a2}\ddot{z}_{a2} + c_{a2}\dot{z}_{a2} + k_{a2}z_{a2} = m_{a2}(\ddot{w_{rel}}(x_l) + \ddot{w}_b) \\ f_{a1} = -[c_{a1}\dot{z}_{a1} + k_{a1}z_{a1}] \\ f_{a2} = -[c_{a2}\dot{z}_{a2} + k_{a2}z_{a2}] \end{cases} \tag{3}$$

where c_{a1} is the damping coefficient of the spring of the resonator 1, and k_{a1} is the stiffness of the spring of the resonator 1. c_{a2} is the damping coefficient of the spring of the electromagnetic part (EM), and k_{a2} is the stiffness of the spring of the electromagnetic part (EM). $\ddot{w}_{rel}(x_a) + \ddot{w}_b$ and $\ddot{w}_{rel}(x_l) + \ddot{w}_b$ is the second derivative of the absolute displacement of the cantilever beam element at resonator 1and at the end of the piezoelectric cantilever respectively.

As shown in Fig. 2(d), the magnetic exciter (MOE) is composed of two rectangular magnets. The approximate expression of rectangular magnetic force f_n is given as follows

$$f_n = \frac{1.5}{1+3d}\frac{whw_{rel}(x_l)}{2\mu_0\sqrt{d^2 + w_{rel}(x_l)^2}} \times \left[\frac{B_r}{\pi}\left(arctan\frac{wh}{2d\sqrt{w^2+h^2+4d^2}} - arctan\frac{wh}{2(d+l)\sqrt{w^2+h^2+4(d+l)^2}}\right]\right. \tag{4}$$

where *l*, *w* and *h* are respectively the length, width and height of the magnet block, μ_0 is the vacuum permeability, $\mu_0 = 4\pi \times 10^{-7} H/m$, B_r is the remanence of the permanent magnet, and the geometric dimensions of the rectangular magnets are shown in Fig. 3 below.

From Fig. 2(d), the equation of motion of the magnet blocks in the magnetic exciter (MOE) is

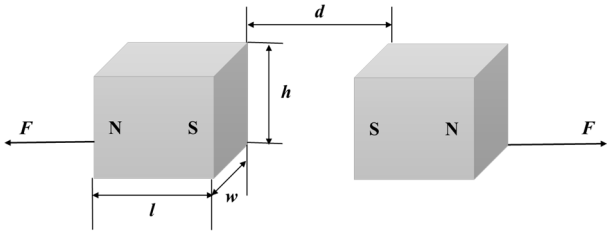

Fig. 3 Schematic diagram of the combined dimensions between rectangular magnets

$$f_m = -f_n + m_s[\ddot{w}_{rel}(x_l) + \ddot{w}_b(t)] \tag{5}$$

where m_s is the mass of the rectangular magnet block, and $\ddot{w}_{rel}(x_l) + \ddot{w}_b$ denotes the second derivative of the absolute displacement at the end of the cantilever.

The electrical properties of the harvester are basically unchanged after the addition of the resonator and the magnetic exciter on the piezoelectric cantilever beam. Therefore, the circuit equations are the same as that of the piezoelectric cantilever beam equation derived in Challa *et al*. (1996).

$$C_p\frac{dV_p}{dt} + \frac{V_p}{R_L} = -\int_0^{l_p} e_{31}z_{pc}b\frac{\partial^3 w_{rel}(x,t)}{\partial x^2 \partial t}dx \qquad C_p = \frac{bl_p\varepsilon_{33}^S}{d_p} \tag{6}$$

where C_p is the equivalent capacitance of the piezoelectric material, R_L is the equivalent resistance, l_p and b are respectively the length and width of the cantilever beam, e_{31} is the piezoelectric constant, z_{pc} is the center coordinates of the piezoelectric chip, d_p is the thickness of the piezoelectric chip, ε_{33}^S is the piezoelectric dielectric constant.

Under the action of external excitation, the magnet oscillates inside the copper coil and causes a change in magnetic flux, thus generating a voltage $V_{em}(t)$ which is given by Lenz's law (Glynne-Jones *et al*. 2004)

$$V_{em}(t) = -\theta_{em}(\dot{z}_{a2} + \dot{w}_{rel}(x_l)) \tag{7}$$

where $\theta_{em} = B_m L_{pc}$ is the electromagnetic coupling coefficient., and B_m is the magnet's flux density, and L_{pc} is the length of the copper coil.

Finally, the power from PHH and EM are given as Eqs. (8) and (9).

$$P_p = \left|\frac{V_p}{\sqrt{2}R_L}\right|^2 R_L \tag{8}$$

$$P_{em} = \left|\frac{V_{em}}{\sqrt{2[R_{em} + R_c]}}\right|^2 R_{em} \tag{9}$$

$$P_{pem} = P_p + P_{em} \tag{10}$$

where the variables P_p, P_{em}, P_{pem} stand for the power harvested of the piezoelectric part, the electromagnetic part,

and the whole device separately.

2.2 Modal superposition method

When the piezoelectric cantilever beam is in operation, it is not only affected by the coupling force of the resonator and the magnetic exciter pair, but also by the reaction force generated by the inverse piezoelectric effect. At this time, the steady-state response of the system can be obtained by modal superposition method.

The relative displacement of each point on the piezoelectric cantilever beam is calculated by modal superposition method (Bennet 1968, Weaver *et al*. 1990)

$$\begin{cases} w_{rel}(x,t) = \sum_{r=1}^{\infty} \hat{\phi}_r(x)\eta_r(t)\ (r = 1,2,3\ldots) \\ \hat{\phi}_r(x) = Q_r[cos\beta_r x - cosh\beta_r x \\ \qquad +\xi_r(sin\beta_r x - sinh\beta_r x)] \end{cases} \tag{11}$$

$$\begin{aligned} &1 + \cos\beta_r l \cosh\beta_r l \\ &+\mu_t\beta_r l(cos\beta_r l sinh\beta_r l - sin\beta_r l cosh\beta_r l) = 0 \end{aligned} \tag{12}$$

$$\xi_r = \frac{sin\beta_r l - \sinh\beta_r l + \mu_t\beta_r l(cos\beta_r l - cosh\beta_r l)}{cos\beta_r l + \cosh\beta_r l - \mu_t\beta_r l(sin\beta_r l - sinh\beta_r l)} \tag{13}$$

where $\eta_r(t)$ is the modal coordinate; $\widehat{\emptyset}_r(x)$ is the mass-normalized mode function; β_r is the characteristic frequency, which can be obtained by Eq. (12); $\mu_t = m_s/\rho_l l$ is the ratio of the end block's mass to the piezoelectric cantilever's mass. Q_r is the modal amplitude constant coefficient. The resonant frequency of the piezoelectric cantilever is given as Eq. (14) according to Eq. (12)

$$\omega_r = (\beta_r l)^2 \sqrt{YI/\rho_l l^4} \tag{14}$$

By using the orthogonal property of modal function (Glynne-Jones *et al*. 2004, Liu *et al*. 2013) and combining with Eq. (2), the expression of $\eta_r(t)$ can be obtained.

$$\begin{aligned} &\ddot{\eta}_r(t) + 2\zeta_r\omega_r\dot{\eta}_r(t) + \omega_r^2\eta_r(t) + \chi_r\theta V_p \\ &= -\gamma_r\rho_l l\ddot{\omega}_b + \hat{\phi}_r(x_a)f_{a1} + \hat{\phi}_r(x_l)f_{a2} + \hat{\phi}_r(x_l)f_m \end{aligned} \tag{15}$$

where the parameter $\zeta_r = \frac{c_s l w_r}{2YI}$ is the damping ratio of the strain rate, $\chi_r = \frac{d\hat{\phi}_r(x)}{dx}\Big|_{x=l}$ is one modal variable, $\gamma_r = Q_r\frac{2\xi_r}{\beta_r l}$ is another modal variable. $\theta = e_{31}bd_p$ is the electromechanical coupling coefficient.

Considering that the second-order resonance frequency is far away from the first-order resonance frequency whose influence on the first-order mode is small (Weaver *et al*. 1990), we only calculate the first-order modal component in the time domain integration. By reducing the order of equation (11) (i.e., r = 1), the above equations of motion and circuit can be sorted out as follows

$$\begin{cases} \ddot{\eta}_1(t) + 2\zeta_1\omega_1\dot{\eta}_1(t) + \omega_1^2\eta_1(t) + \chi_1\theta V_p = -\gamma_1\rho_l l\ddot{w}_b + \hat{\phi}_1(x_a)f_{a1} + \hat{\phi}_1(x_l)f_{a2} + \hat{\phi}_1(x_l)f_m \\ m_{a1}\ddot{z}_{a1} + c_{a1}\dot{z}_{a1} + k_{a1}z_{a1} = m_{a1}(\hat{\phi}_1(x_a)\ddot{\eta}_1(t) + \ddot{w}_b) \\ m_{a2}\ddot{z}_{a2} + c_{a2}\dot{z}_{a2} + k_{a2}z_{a2} = m_{a2}(\hat{\phi}_1(x_l)\ddot{\eta}_1(t) + \ddot{w}_b) \\ f_{a1} = -[c_{a1}\dot{z}_{a1} + k_{a1}z_{a1}] \\ f_{a2} = -[c_{a2}\dot{z}_{a2} + k_{a2}z_{a2}] \\ f_m = -f_n + m_s[\hat{\phi}_1(x_l)\ddot{\eta}_1(t) + \ddot{w}_b] \\ C_p\frac{dV_p}{dt} + \frac{V_p}{R_L} = -\chi_1 e_{31}z_{pc}b\dot{\eta}_1(t) \\ V_{em}(t) = -\theta_{em}(\dot{z}_{a2} + \dot{w}_{rel}(x_l)) \end{cases} \tag{16}$$

By solving the Eq. (16), the time-domain solutions of the output voltages of PE and EM are obtained, and the power harvested by PE, EM and BMHEH is obtained by introducing Eqs. (8), (9) and (10).

2.3 Solution of using the Runge-Kutta algorithm

Because of the existence of nonlinear magnetic force in BMHEH, it is difficult to get the analytical solution of the output voltage. But the numerical solution of the motion equation and circuit equation can be obtained by means of time domain integration, using the Runge-Kutta algorithm (Lu *et al*. 1996) which can get higher precision results. Since the algorithm is suitable for solving first-order differential equations, it is necessary to introduce intermediate variables to reduce the order of Eq. (16). The calculation process is as follows:

The following intermediate variables are introduced

$$\begin{cases} x_\eta(t) = \dot{\eta}_1(t) \\ x_{za1}(t) = \dot{z}_{a1}(t) \\ x_{za2}(t) = \dot{z}_{a2}(t) \end{cases} \tag{17}$$

The differential equation of Eq. (16) can be reduced to the first-order differential equation and expressed as

$$\begin{cases} \dot{x}_\eta(t) = \dfrac{-\gamma_1\rho_l l\ddot{w}_b - m_s\hat{\phi}_1(x_l)\ddot{w}_b - (2\zeta_1\omega_1 x_\eta(t) + +\omega_1^2\eta_1(t) + \chi_1\theta V_p - \hat{\phi}_1(x_a)(c_{a1}x_{za1}(t) + k_{a1}z_{a1}) - \hat{\phi}_1(x_l)(c_{a2}x_{za2}(t) + k_{a2}z_{a2})}{1 - m_s\hat{\phi}_1(x_l)^2} \\ \dot{\eta}_1(t) = x_\eta(t) \\ \dot{x}_{za1}(t) = \ddot{w}_b + \hat{\phi}_1(x_a)\dot{x}_\eta(t) - \dfrac{c_{a1}x_{za1}(t) + k_{a1}z_{a1}}{m_{a1}} \\ \dot{z}_{a1}(t) = x_{za1}(t) \\ \dot{x}_{za2}(t) = \ddot{w}_b + \hat{\phi}_1(x_l)\dot{x}_\eta(t) - \dfrac{c_{a2}x_{za2}(t) + k_{a2}z_{a2}}{m_{a2}} \\ \dot{z}_{a2}(t) = x_{za2}(t) \\ \dot{V}_p = -\dfrac{V_p}{R_L C_p} - \chi_1 e_{31} z_{pc} b x_\eta(t) \Big/ C_p \\ V_{em}(t) = -\theta_{em}(x_{za2}(t) + \hat{\phi}_1(x_l)x_\eta(t)) \end{cases} \tag{18}$$

By using the fourth-order Runge-Kutta algorithm to solve the reduced-order Eq. (18), the analytical solution of the frequency response function of the output voltage can be obtained, and the frequency-domain solution of the system power can be received in the case of sweeping frequency excitation input.

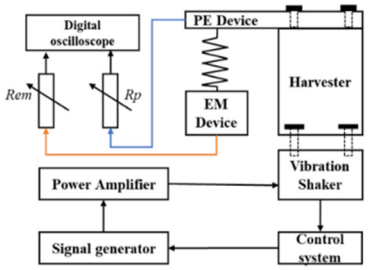

(a) Schematic diagram of experimental setup

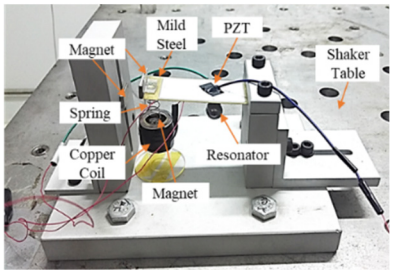

(b) Details of the experimental equipment

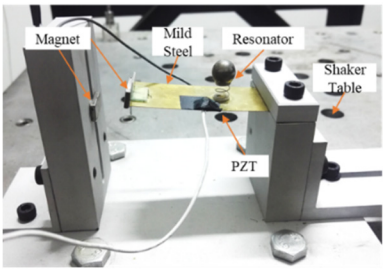

(c) Independent piezoelectric portion

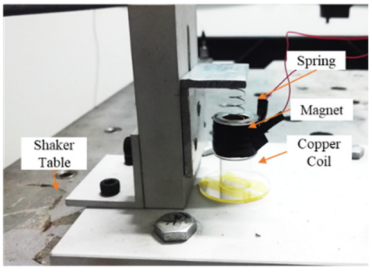

(d) Independent electromagnetic portion

Fig. 4 Detailed illustration of experimental equipment

Table 1 Parameters of the experimental device

Parameter	Value	Parameter	Value
Length of the beam-l	80×10^{-3} m	Permittivity-ε_{33}^{S}	15.93 nF/m
Width of the beam-b	33×10^{-3} m	Equivalent resistance of the PZT-R_L	$500\times10^{3}\Omega$
Thickness of the beam-d	0.6×10^{-3} m	Mass of the block magnet-m_t	4.0×10^{-3} kg
Thickness of the metal base-d_b	0.4×10^{-3} m	Length of the block magnet-l_t	20×10^{-3} m
Thickness of the PZT-d_p	0.2×10^{-3} m	Width of the block magnet-w_t	10×10^{-3} m
Density of the base-ρ_b	8900 kg/m^3	Thickness of the block magnet-h_t	3×10^{-3} m
Density of the PZT-ρ_p	7800 kg/m^3	Residual magnetic flux of the rectangular magnet-Br	1.25 T
Young's modulus of the PZT-Y_p	66 GPa	Mass of the cylindrical magnet-m_s	8.0×10^{-3} kg
Young's modulus of the base-Y_b	96 GPa	Residual magnetic flux of the cylindrical magnet-B_s	1.1 T
Piezoelectric constant-e_{31}	-12.54 N/mV	Equivalent resistance of coils-R_{em}	500 Ω
Stiffness of the EM harvester-K_{a2}	38.2 N/m	Mass of the resonator mass block-m_a	8.0×10^{-3} kg
Damping ratio of the PZT-ζ	0.01	Stiffness of the resonator spring-k_{a1}	613 N/m
Damping ratio of the resonator spring-ζ_{a1}	0.0055	Damping ratio of the EM harvester-ζ_{a2}	0.0044

3. Construction of BMHEH experimental test platform

The amount of power and voltage captured by the hybrid energy harvester is verified and evaluated experimentally. Fig. 4(a) shows the simplified block diagram of the experimental system. Fig. 1(b) shows the physical diagram of the experimental system. The system is mainly composed of a hybrid energy harvester, an electromagnetic vibration table, a digital oscilloscope, a resistor box, circuits, and a digital voltmeter. The piezoelectric cantilever's substrate is made of copper (density 8900 kg/m^3, elastic modulus 96 GPa) and piezoelectric ceramic (PZT-5A, density 7800 kg/m^3, elastic modulus 66 GPa), and the dynamic resonator is a spring-mass vibration subsystem. The material of the permanent magnet is N35. The cylindrical permanent magnet N35 is suspended by a spring and moves up and down inside the electromagnetic coil (copper coil). The whole device is fixed on the shaker, and the resistance box is used as the load resistance. The output voltage can be measured across the load resistors. The digital oscilloscope can record the voltage and other data captured by the BMHEH vibration generator in real time. All values related to the experiment are shown in Table 1.

To measure and assess the power generation performance of the hybrid energy harvester, it was compared to the independent piezoelectric and electromagnetic energy harvester respectively. The independent piezoelectric energy portion is shown in Fig. 4(c), and the independent electromagnetic energy portion is shown in Fig. 4(d). The parameters of the hybrid energy harvester are the same as the piezoelectric and electromagnetic portions of the hybrid energy harvester, respectively.

4. Experimental results and analysis

4.1 Experimental and analytical study

This section analyzes the maximum output power of the hybrid harvester and compares it with the output power value of the independent piezoelectric and electromagnetic portion. The experimental results and numerical simulation results of the hybrid energy harvester and the independent portion are compared and analyzed. The experiment and simulations are carried out under the base harmonic excitation by an electromagnetic shaker mount. The amplitude λ of the harmonic excitation is 1 mm, the acceleration a is 3 m/s^2 and the frequency ($f = \omega/2\pi$) is varied from 5 Hz to 50 Hz.

In the BMHEH system, the external loads of the piezoelectric system and the electromagnetic system are R_L and R_{em} respectively (in Fig. 5). Resistance across PE and EM circuit is varied in the range of 10–200 KΩ and 0~1250 Ω respectively. The output voltages are measured by voltmeter and the maximum output power can be then obtained. The experimental results are shown in Fig. 5 below.

Figs. 5(a) and (b) respectively represent the power of the independent piezoelectric or electromagnetic energy harvester. Figs. 5(c) and (d) respectively represent the curves of the power collected by the piezoelectric portion and the electromagnetic portion as a function. According to Figs. 5(a), (c) and 5(b), (d): the optimum load resistance of the piezoelectric portion and the electromagnetic portion circuits are respectively about 60 KΩ and 550 Ω. From the experimental results, the optimal resistance of both circuits is basically unchanged for the independent and hybrid energy harvesters, so these values (RL = 60 kΩ and Rem = 550 Ω) can be used for the theoretical analysis.

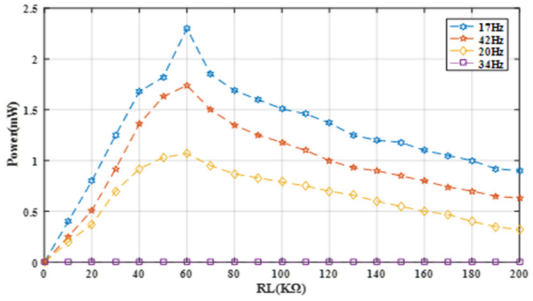

(a) Power with RL in independent piezoelectric device

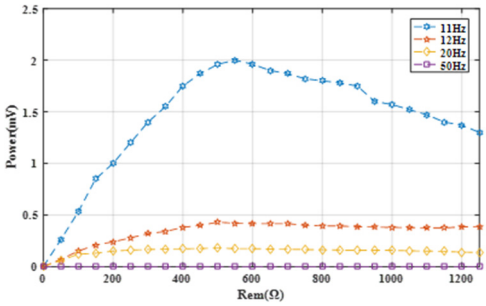

(b) Power with R_{em} in independent piezoelectric device

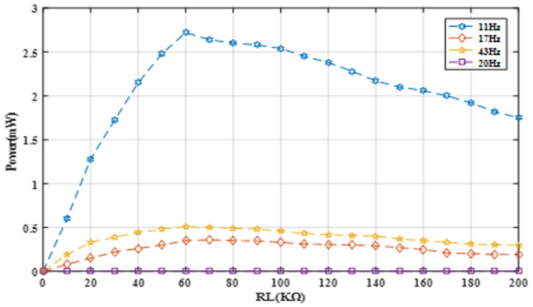

(c) Power with RL in hybrid piezoelectric device

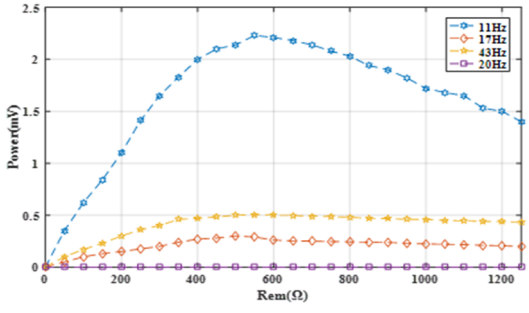

(d) Power with Rem in hybrid piezoelectric device

Fig. 5 Output power response of different resistances

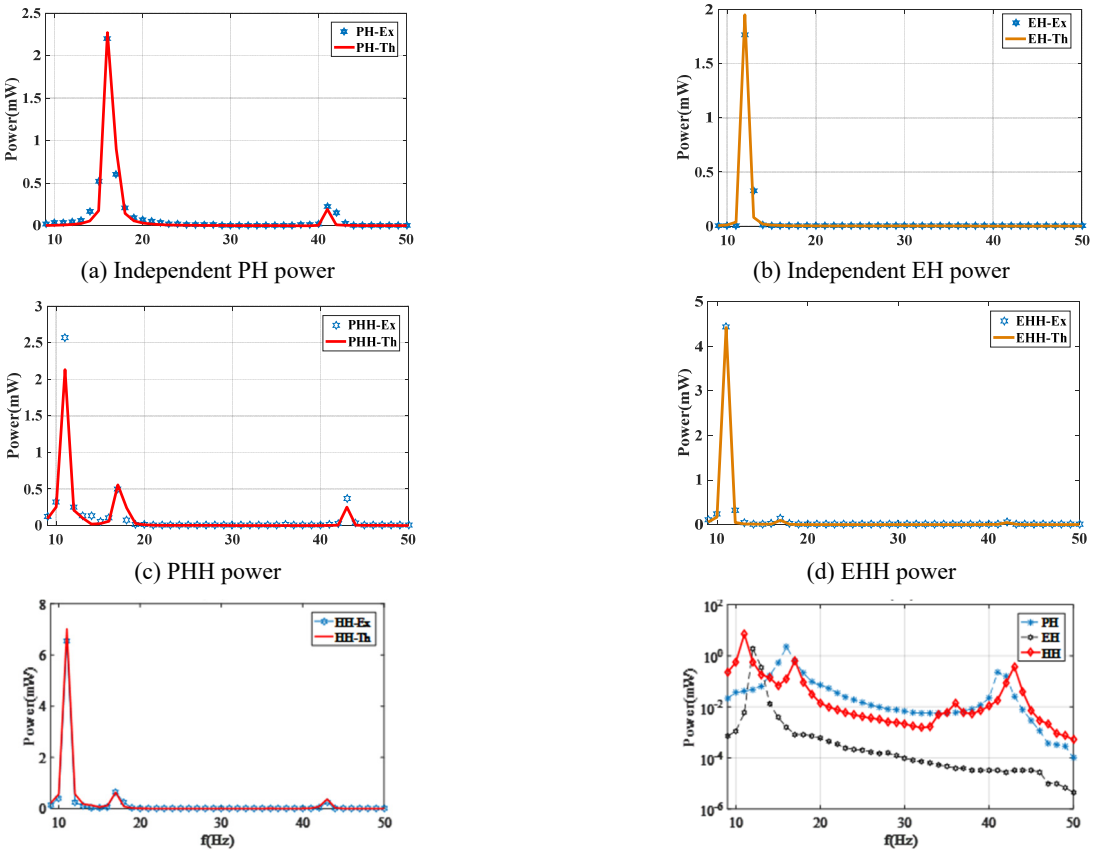

(a) Independent PH power

(b) Independent EH power

(c) PHH power

(d) EHH power

(e) Comparison of independent HH

(f) PH power, independent EH and HH powers

Fig. 6 Comparison of output power in experiments (Ex) and simulations (Th)

Table 2 Results comparison of the independent and hybrid energy harvesters

Type frequencies and peak power	Independent piezoelectric (PH)	Independent electromagnetic (EH)	Piezoelectric part of BMHEH (PHH)	Electromagnetic part of BMHEH (EHH)	Hybrid harvester (BMHEH)
The first (Hz)	18	11	11	11	11
Value 1 (mW)	2.22	1.81	2.63	4.27	6.92
The second (Hz)	43	-	17	17	17
Value 2 (mW)	0.21	-	0.62	0.02	0.64
The third (Hz)	-	-	42	42	42
Value 3 (mW)	-	-	0.21	0.001	0.211

As can be seen from Fig. 6(a): the output power of an independent piezoelectric portion (PH) reaches peaks at around 18 Hz and 43 Hz, which are the resonance frequencies of the independent piezoelectric due to the coupling of piezoelectric parts, and the resonator respectively, and Fig. 6(b) shows the output power of an independent electromagnetic energy harvester (EH) peaks at around 11 Hz, which is its resonant frequency. Fig. 6(c), (d) and (e) show that the frequencies corresponding to the peak output power of PHH, EHH and HH are close to 11 Hz, 17 Hz, and 42 Hz. Compared to an independent energy harvester, the resonance frequencies of the hybrid harvester decrease, the frequency band of energy collection is broadened, and the collected power is also improved over an independent energy harvester. Fig. 6(f) compares experimental power of independent piezoelectric, independent electromagnetic and hybrid harvesters. And first-order resonance frequency of the broadband-multimodal hybrid energy harvester (BMHEH) is lower than that of an independent energy harvester and the hybrid harvester power exceeds the independent power in a large area between the two resonant frequencies. Therefore, the wideband and low-frequency power generated by the hybrid harvester cannot be realized by independent devices. Table 2 shows the results comparison of the independent and hybrid energy harvesters.

Figs. 6(a)-(e) show the resonance frequency obtained by the theoretical model is very close to that obtained by the experimental data, which has verified both the simulation and the experimental results in a certain precision. Hence, all subsequent analyses can be based on simplified theoretical models.

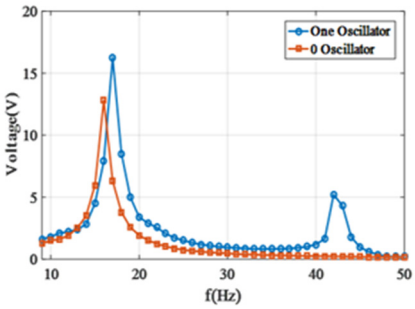

(a) The influence of resonator on the frequency band of the system

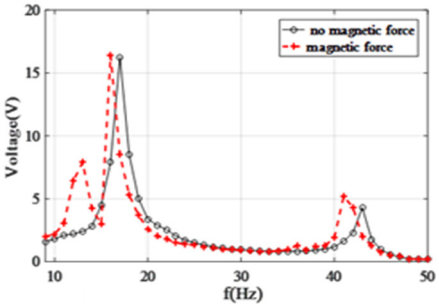

(b) The influence of nonlinear magnetic force on the frequency band of the system

Fig. 7 Influence of resonator and nonlinear magnetic force on frequency band of system

From Fig. 7(a), comparing the voltage curves under the experimental conditions of the resonator and the non-resonator, it can be observed that after adding a resonator to an independent piezoelectric energy harvester, the resonance frequency will increase, and the modal order will be correspondingly increased. The natural frequency of the cantilever beam and the resonator are about 17 Hz and 43 Hz respectively. The resonator only has a great influence on the vibration mode which is close to its own resonance frequency. In Fig. 7(b), the voltage response under two configurations with or without a nonlinear magnetic force is compared. The magnetic pairs in the MOE are attracted to each other. The voltage response of the device with MOE has three peaks, while the voltage response of the device without MOE has only two peaks. Moreover, the output voltage's peak value of the harvester with MOE is higher than that of the harvester without MOE, but the resonant frequency is lower than the resonant frequency of the harvester without MOE. It is fully proved that the introduction of nonlinear magnetic force not only broadens the bandwidth and improves the output performance, but also changes the resonance frequency of the system. The main reason is that the configuration of the permanent magnet attraction (repulsion) reduces (enhances) the system stiffness and changes the resonance frequency of the system (Challa *et al*. 1996). In addition to broadening the bandwidth and improving performance, the two types of attraction and rejection of the magnetic pair will affect the

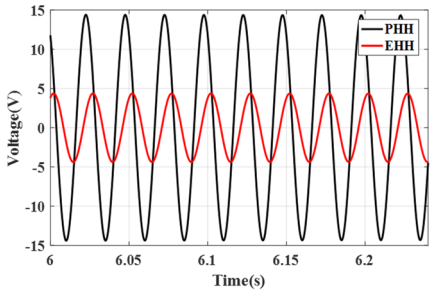

(a) Voltage of PHH and EHH

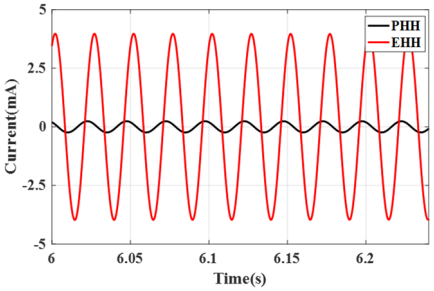

(b) Current of PHH and EHH

Fig. 8 Recorded voltage and current time history response of BMHEH.

Table 3 Comparison of volume, power and energy density of different energy harvesters

Parameter type	Ref.	Volume (cm^3)	Mass (g)	Resonance (Hz)	Voltage (V)	Current (mA)	Power density ($\mu W/cm^3$)
EH	Glynne-Jones *et al*. (2004)	0.84	-	322	0.0094	7.85	44.05
EH	Liu *et al*. (2013)	0.035	0.0352	840	0.0037	0.00296	0.157
PH	Roundy and Wright (2004)	1.00	-	120	12.54	0.06	375
PH	Sari *et al*. (2008)	3.52	20.6	45.6	4.17	0.12	70.6
PH	Zhao and Erturk (2009)	4.43	23.8	-	13.65	0.0014	2.12
HH	Ab Rahman *et al*. (2013)	-	44.3	21.6	2.55(PHH) 0.099(EHH)	0.073(PHH) 1.46(EHH)	9.5
This work		7.3	43.2	11,17,43	16.67(PHH) 2.66(EHH)	0.28(PHH) 3.12(EHH)	756.5

resonance frequency of the system to some extent. If the magnetic pairs of the end magnets are arranged in a mutual attraction/repulsion mode, the soft/hard elastic system is formed, which reduces or improves the stiffness of the system, thereby reducing or increasing the resonance frequency of the system.

It can be seen from Figs. 8(a) and (b) that the output voltage and output current of PHH, EHH vary with time when the harvester base is at a harmonic amplitude of 1 mm and a frequency of 11 Hz. It indicates that the system reaches a steady state and can stably output electric energy. The voltage curves (Fig. 8(a)) show that the output voltage's peak value of PHH is about 4 times that of EHH. The current curves (Fig. 8(b)) show that the output current's peak value of EHH is 30 times that of PHH. Therefore, the hybrid harvester can produce high voltage and current at the same time. In order to illustrate the advantages of the hybrid harvester, it is compared with the existing piezoelectric and electromagnetic harvesters. Table 3 reports harvesters with the resonance frequency, volume and power harvesting capacity from papers.

From Table 3, the results show that the hybrid harvester has higher power density and more resonant frequencies. Further, the resonant frequency of the harvester is low, which is suitable for low frequency applications. It is proved that the proposed hybrid energy harvester is more suitable for the wide frequency and multimodal energy collection.

4.2 Numerical analysis study

Numerical studies are used to determine the effect of the mass and spring stiffness of the resonator, as well as the magnet block at the end on the bandwidth and collection power of the energy harvester. Figs. 9(a), (b), (c), and (d) illustrate the effects of the mass and spring stiffness of the resonator on the bandwidth and power of the harvester.

It can be observed from Figs. 9(a) and (c) that the second and third resonance frequencies decrease to some extent and the output voltage is properly raised with the increase of resonator mass, which is suitable for the energy collection of the low frequency vibration structure. Three resonance frequencies are gradually approaching, and the frequency band of action is also decreasing. It can be observed from Figs. 9(b) and (d) that the effect of the spring stiffness of the resonator is more in the third resonating frequency. As the stiffness increases, the second and third resonant frequencies of the system increase, the resonating frequencies are more separated from each other, and the frequency bandwidth of the three modes does not changes much but the output voltage peak values of the second and third modes are somewhat reduced.

Comparing with Figs. 10(a), (c), (b) and (d), it can be implied that the electromechanical coupling coefficient θ and the electromagnetic coupling coefficient θ_{em} significantly affect the output voltage and peak of output-power obviously but have little effect on the resonance frequency. Therefore, the electromechanical coupling coefficient and the electromagnetic coupling coefficient significantly will increase the output voltage and output-power peak values and harvesting frequency bandwidth of the system.

From Figs. 11(a) and (c), it can be concluded that the mass of the end magnet mainly affects the second and third resonance frequencies of the energy harvester. With the increase of mass, the third resonance frequency decreases, and the resonant frequencies move closer to each other. As the total power increases and the bandwidth of the near second resonance frequency decreases, thereby the device is suitable for the environment with low frequencies vibration characteristics, such as bridges and buildings. It can be seen from Figs. 11(b) and (d) that the magnetic flux has a significant influence on the three resonant frequencies of the harvester. As the magnetic flux increases, the number of

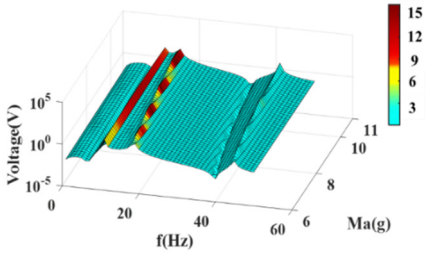

(a) Voltage of PHH and EHH

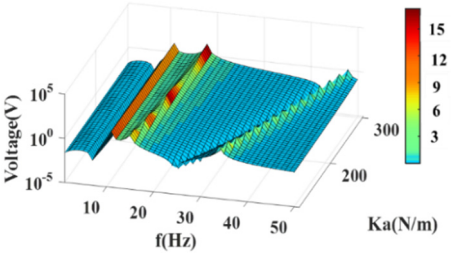

(b) Current of PHH and EHH

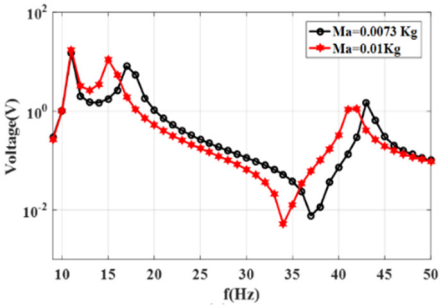

(c) Two kinds of resonator mass

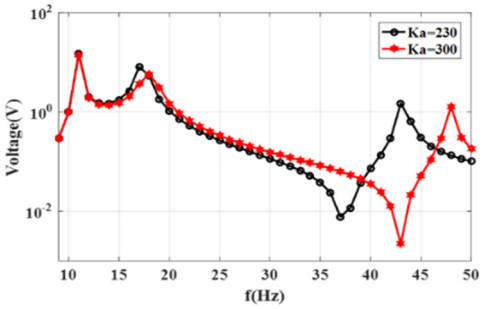

(d) Two kinds of spring stiffness

Fig. 9 The effects of the mass and stiffness of the resonator on the bandwidth and power of the harvester

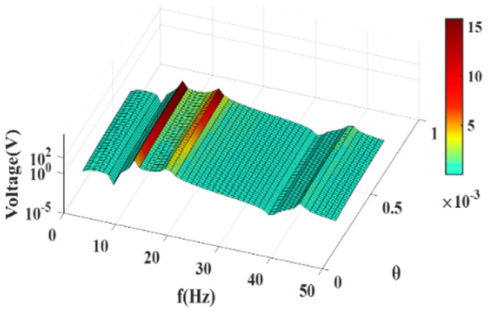

(a) Voltage of PHH and EHH

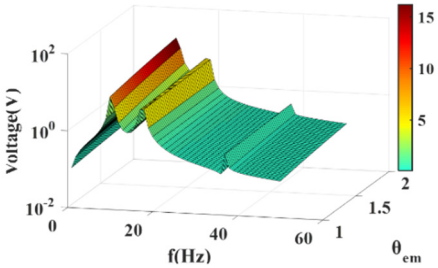

(b) Current of PHH and EHH

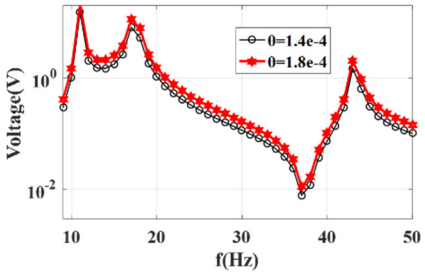

(c) Two θ values

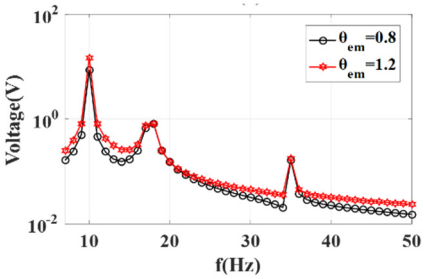

(d) Two θ_{em} values

Fig. 10 Effect of electromechanical coupling coefficient and electromagnetic coupling coefficient on the bandwidth and output voltage of the harvester

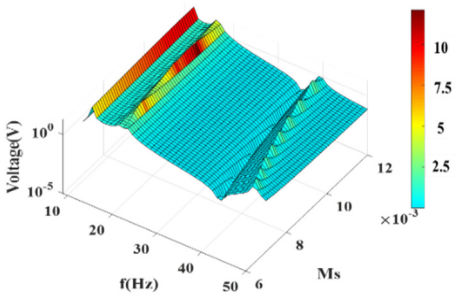

(a) The effect of magnet mass

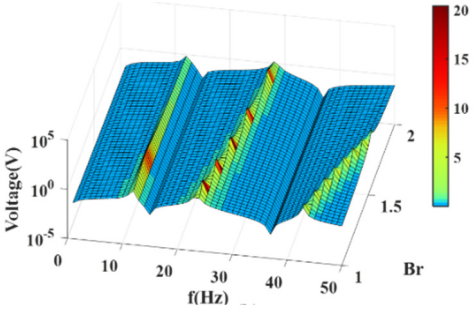

(b) The effect of magnetic flux intensity

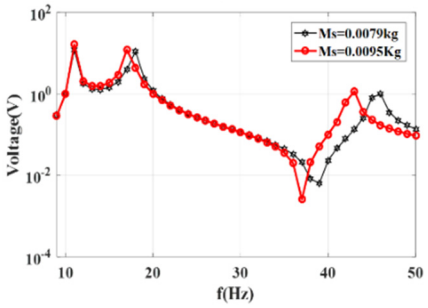

(c) The two magnet mass sample values

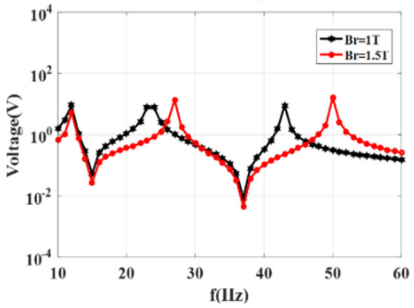

(d) The two magnetic flux intensity sample values

Fig. 11 Effect of mass and flux of rectangular magnet at the end of collector on bandwidth and output voltage

resonance frequencies increases, the frequency band widens gradually and the output voltage increases to a certain extent. If the magnetic field is strong, it affects the resonant frequencies and generates the nonlinear effects. If the magnetic field is weak, it affects the resonant frequencies very little. The large magnetic flux intensity will increase the harvesting bandwidth.

Therefore, under a certain regulation range, the effects of the mass and spring stiffness of the resonator, as well as the electromechanical and electromagnetic coupling coefficients, magnet mass and magnetic flux intensity and many other factors on the response bandwidth and output power are shown in Table 4 below.

Table 4 The influence of various factors on the bandwidth and output power of the system

Factor	Bandwidth	Output power
Resonator mass M_a↑	Appropriately decrease ↓	Increase ↑
Spring stiffness K_a↑	Increase ↑	Decrease within a certain range ↓
Electromechanical coupling- coefficient θ ↑	Minor effect	Appropriately increase ↑
Electromagnetic coupling- coefficient θ_{em}↑	Minor effect	Appropriately increase ↑
Magnet mass M_s ↑	Appropriately decrease ↓	Appropriately increase ↑
Magnetic flux B_r↑	Increase ↑	Appropriately increase ↑

5. Conclusions

An improved continuum electromechanical coupling analytical model was proposed for a new type of broadband-multimode piezoelectric-electromagnetic hybrid vibration energy harvester in this paper. The nonlinear model was solved by the Runge-Kutta algorithm, and the following conclusions are obtained through experimental verification and numerical simulation.

- The resonator can not only increase the modal number of the hybrid harvester, but also adjust the resonance frequency of the harvester, and increase the bandwidth. The introduction of the nonlinear magnetic force can adjust the resonance frequency, widen the frequency band and improve the output performance. Thus, the harvester has strong flexibility.
- The hybrid energy harvester can simultaneously generate high voltage and high current characteristics. The peak output voltage of the piezoelectric part is about 4 times that of the electromagnetic part, and the peak output current of the electromagnetic part is about 30 times that of the piezoelectric part.
- It can be observed that the proposed harvester possesses higher power density and more resonant frequencies compared to the existing piezoelectric and electromagnetic harvesters. Also, the harvester has a low resonant frequency which is suitable for low frequency applications. It is proven that the hybrid is more suitable for the wide frequency band and multimodal energy collection.
- The bandwidth of frequency can be adjusted by changing the stiffness and magnetic flux intensity of the resonator. The energy collected by the system can be adjusted within a certain range by the mass of the resonator, the electromechanical coupling coefficient, the electromagnetic coupling coefficient, and the mass of the magnet block.

This study proved that the hybrid energy harvester is an effective method to improve the output performance and bandwidth of the traditional piezoelectric vibration energy harvester from both theoretical and experimental aspects. However, the device has not been analyzed from an optimization perspective and needs further study.

Acknowledgments

This work is supported by the Fundamental Research Funds for the Central Universities **(FRF-GF-19-009B)** and University of Science and Technology Beijing. Useful discussions with Professor **Zhongjun Yin** at the University of Science and Technology Beijing, is also gratefully acknowledged.

References

Ab Rahman, M.F., Kok, S.L., Ali, N.M., Hamzah, R.A. and Aziz, K.A.A. (2013), "Hybrid vibration energy harvester based on piezoelectric and electromagnetic transduction mechanism", *Proceedings of 2013 IEEE Conference on Clean Energy and Technology* (*CEAT*), Langkawi, Malaysia, November, pp. 243-247. https://doi.org/10.1109/CEAT.2013.6775634

Lu, L.-H., Nakagawa, R., Kashio, Y., Ito, A., Shoji, H., Nishi, N., Hirashima, M., Yamauchi, A. and Nakamura, T. (1996), "Dynamical systems and numerical analysis", *IEEE Computat. Sci. Eng.*, **4**(2), 86-87. https://doi.org/10.1109/MCSE.1997.609839

Ali, S.F., Friswell, M.I. and Adhikari, S. (2010), "Piezoelectric energy harvesting with parametric uncertainty", *Smart Mater. Struct.*, **19**(10), 105010-105019. https://doi.org/10.1088/0964-1726/19/10/105010

Beeby, S.P., Tudor, M.J. and White, N.M. (2006), "Energy harvesting vibration sources for microsystems applications", *Measure. Sci. Technol.*, **17**(12), 175-195. https://doi.org/10.1088/0957-0233/17/12/r01.

Bennet, A.G. (1968), *Electricity and Modern Physics*, London: Edward Arnold, London, UK.

Cannarella, J., Selvaggi, J., Salon, S., Tichy, J. and Borca-Tasciuc, D.A. (2011), "Coupling factor between the magnetic and mechanical energy domains in electromagnetic power harvesting applications", *IEEE Transact. Magnet.*, **47**(8), 2076-2080. https://doi.org/10.1109/TMAG.2011.2122265

Challa, V.R., Prasad, M.G., Shi, Y. and Fisher, F.T. (1996), "A vibration energy harvesting device with bidirectional resonance frequency tenability", *Smart Mater. Struct.*, **17**(1), 15035-15010. https://doi.org/10.1088/0964-1726/17/01/015035

Erturk, A. and Inman, D.J. (2008), "A distributed parameter electromechanical model for cantilevered piezoelectric energy harvesters", *J. Vib. Acoust.-Transact. ASME*, **130**(4). https://doi.org/041002-041017. 10.1115/1.2890402

Erturk, A., Hoffmann, J. and Inman, D.J. (2009), "A piezomagnetoelastic structure for broadband vibration energy harvesting", *Appl. Phys. Lett.*, **94**(25), 254102-254105. https://doi.org/10.1063/1.3159815

Glynne-Jones, P., Tudor, M.J., Beeby, S.P. and White, N.M.

(2004), "An electromagnetic, vibration powered generator for intelligent sensor systems", *Sensors Actuat. A: Phys.*, **110**(1), 344-349. https://doi.org/10.1016/j.sna.2003.09.045

Hannan, M.A., Mutashar, S., Samad, S.A. and Hussain, A. (2014), "Energy harvesting for the implantable biomedical devices: issues and challenges", *BioMed. Eng. Online*, **13**(1), 79-102. https://doi.org/10.1186/1475-925X-13-79

Huang, S.C. and Lin, K.A. (2012), "A novel design of a map-tuning piezoelectric vibration energy harvester", *Smart Mater. Struct.*, **21**(8), 085014-085024. https://doi.org/10.1088/0964-1726/21/8/085014

Jaber, N., Ramini, A., Hennawi, Q. and Younis, M.I. (2016), "Wideband MEMS resonator using multifrequency excitation", *Sensors Actuat A: Phys.*, **106**(2015), 140-145. https://doi.org/10.1016/j.sna.2016.02.030

Kumar, K.A., Ali, S.F. and Arockiarajan, A. (2015), "Piezomagnetoelastic broadband energy harvester: Nonlinear modeling and characterization", *Eur. Phys. J. Special Topics*, **224**(14-15), 2803-2822. https://doi.org/10.1140/epjst/e2015-02590-8

Leng, Y., Tan, D., Liu, J., Zhang, Y. and Fan, S. (2017), "Magnetic force analysis and performance of a tri-stable piezoelectric energy harvester under random excitation", *J. Sound Vib.*, **406**, 146-160. https://doi.org/10.1016/j.jsv.2017.06.020

Liu, H., Qian, Y. and Lee, C. (2013), "A multi-frequency vibration-based mems electromagnetic energy harvesting device", *Sensors Actuat. A: Phys.*, **204**(24), 37-43. https://doi.org/10.1016/j.sna.2013.09.015

Mann, B.P. and Sims, N.D. (2009), "Energy harvesting from the nonlinear oscillations of magnetic levitation", *J. Sound Vib.*, **319**(1-2), 515-530. https://doi.org/10.1016/j.jsv.2008.06.011

Matiko, J.W., Grabham, N.J., Beeby, S.P. and Tudor, M.J. (2013), "Review of the application of energy harvesting in buildings", *Measure. Sci. Technol.*, **25**(1), 012002-012027. https://doi.org/10.1088/0957-0233/25/1/012002

Mutashar, S., Hannan, M.A., Samad, S.A. and Hussain, A. (2013), "Efficient low-power recovery circuits for bio-implanted micro-sensors", Przeglad zachodni. 89(5), 15-18.

Rajarathinam, M. and Ali, S.F. (2018), "Energy generation in a hybrid harvester under harmonic excitation", *Energy Convers. Manage.*, **155**, 10-19. https://doi.org/10.1016/j.enconman.2017.10.054

Roundy, S. and Wright, P.K. (2004), "A piezoelectric vibration based generator for wireless electronics", *Smart Mater. Struct.*, **13**(5), 1131-1142. https://doi.org/10.1088/0964-1726/13/5/018

Sari, I., Balkan, T. and Kulah, H. (2008), "An electromagnetic micro power generator for wideband environmental vibrations", *Sensors Actuat. A: Phys.*, **145**, 405-413. https://doi.org/10.1016/j.sna.2007.11.021

Shen, W., Chen, D., Li, L. and Tao, M. (2015), "Modeling and simulation of vibration energy harvester with piezomagnetoelastic beam array", *Proceedings of 2015 IEEE 19th International Conference on Computer Supported Cooperative Work in Design* (*CSCWD*), Calabria, Italy, May, pp. 303-307. https://doi.org/10.1109/CSCWD.2015.7230976

Siddique, A.R.M., Mahmud, S. and Van Heyst, B. (2015), "A comprehensive review on vibration based micro power generators using electromagnetic and piezoelectric transducer mechanisms", *Energy Convers. Manage.*, **106**, 728-747. https://doi.org/10.1016/j.enconman.2015.09.071

Tao, K., Ding, G.F., Wang, P.H., Liu, Q.F. and Yang, Z.Q. (2011), "Design and Simulation of Fully Integrated Micro Electromagnetic Vibration Energy Harvester", *Appl. Mech. Mater*, **152**, 1087-1090. https://doi.org/10.4028/www.scientific.net/amm.152-154.1087

Varoto, P.S. and Mineto, A.T. (2014), "Nonlinear Dynamic Behavior of Cantilever Piezoelectric Energy Harvesters: Numerical and Experimental Investigation", In: *Structural Health Monitoring*, Proceedings of the Society for Experimental Mechanics Series, Bethel, CT, USA.

Wang, X. (2016), *Frequency Analysis of Vibration Energy Harvesting Systems*, Elsevier, London, UK.

Wang, X. and Xiao, H. (2013). "Dimensionless analysis and optimization of piezoelectric vibration energy harvester", *Int. Review Mech. Eng.*, **7**(4), 607-624.

Weaver Jr, W., Timoshenko, S.P. and Young, D.H. (1990), *Vibration Problems in Engineering*, John Wiley & Sons, **208**(5014), 417-432. https://doi.org/10.1038/208964b0

Yang, B., Lee, C., Xiang, W., Xie, J., He, J.H., Kotlanka, R.K., Low, S.P. and Feng, H. (2009), "Electromagnetic energy harvesting from vibrations of multiple frequencies", *J. Micromech. Microeng.*, **19**(3), 035001. https://doi.org/035001-035009.10.1088/0960-1317/19/3/035001

Zhao, S. and Erturk, A. (2009), "On the stochastic excitation of monostable and bistable electroelastic power generators: Relative advantages and tradeoffs in a physical system", *Appl. Phys. Lett.*, **102**(10), 1867-1897. https://doi.org/1867-1897.10.1063/1.4795296

Zhao, S. and Erturk, A. (2013), "Electroelastic modeling and experimental validations of piezoelectric energy harvesting from broadband random vibrations of cantilevered bimorphs", *Smart Mater Struct.*, **22**(1), 015002-015016. https://doi.org/10.1088/0964-1726/22/1/015002

Zhou, W., Penamalli, G.R. and Zuo, L. (2011), "An efficient vibration energy harvester with a multi-mode dynamic magnifier", *Smart Mater. Struct.*, **21**(1), 015014-015023. https://doi.org/10.1088/0964-1726/21/1/015014

Zhou, S., Cao, J., Inman, D.J., Lin, J. and Li, D. (2016), "Harmonic balance analysis of nonlinear tristable energy harvesters for performance enhancement", **373**, 223-235. https://doi.org/10.1016/j.jsv.2016.03.017

CC